J Solid State Electrochem (2011) 15:1201–1207
DOI 10.1007/s10008-010-1192-8

ORIGINAL PAPER

Barrier and semiconducting properties of thin anodic films on chromium in an acid solution

Željka Petrović · Nushe Lajçi · Mirjana Metikoš-Huković · Ranko Babić

Received: 28 May 2010 / Revised: 31 July 2010 / Accepted: 4 September 2010 / Published online: 17 September 2010

Abstract The study of barrier and semiconducting properties of anodically formed oxide films on chromium in an acid solution was carried out using the Cr-quartz crystal electrode. The oxide film formation and growth occur through an anion vacancies transport via a low-field-assisted mechanism ($H=10^6$ V cm^{-1}). The anion diffusion coefficient, which quantitatively describes the transport of point defects within the growing film, was calculated from capacitance data using the Nernst-Planck equation for low-field limit approximation and Mott-Schottky analysis. The depletion region in the passive film, close to the film| electrolyte interface, dominates the semiconducting properties. The passive film on Cr in an acid solution behaves as an n-type semiconductor. An energy-band structure model of the passive film is given.

Keywords Chromium-quartz crystal electrode · Chromium hydrated oxide · Low-field mechanism · Diffusion coefficient of anion vacancies · N-type semiconductor

List of symbols

A	Area of the electrode (cm^2)
c	Concentration (mol dm^{-3})
C	Capacitance (F cm^{-2})
C_{SC}	Space charge capacitance (F cm^{-2})
CPE	Constant phase element
D_O	Diffusivity of oxygen vacancies (cm^2 s^{-1})
e	Electron charge (1.602×10^{-19} C)
E	Potential (V)
E_f	Film formation potential (V)
E_C, E_V	Conduction (valence) band edge of semiconductor
E_F	Fermi level
E_{fb}	Flat-band potential of semiconductor (V)
f	Frequency (Hz)
f_c	Characteristic frequency (Hz)
F	Faraday constant (96,500 C mol^{-1})
H	Electric field strength (V cm^{-1})
j	Current density (A cm^{-2})
J_O	Steady state flux of oxygen vacancies (s^{-1} cm^{-2})
jω	Complex variable for sinusoidal perturbations with $\omega = 2f\pi$
k	Boltzman constant (1.38×10^{-23} J K^{-1})
L_{ss}	Layer thickness (nm)
M_i	Molar mass of a species i (g mol^{-1})
N_D	Donor concentration (cm^{-3})
n	Number of electrons interchanged
p	Concentration of holes
Q	Constant of the CPE (Ω^{-1} cm^{-2} s$^{\alpha}$)
Q	Charge (C cm^{-2})
R	Resistance (Ω cm^2)
R_{el}	Solution resistance (Ω cm^2)
T	Temperature (°C)
t	Time (s)
V	Molar volume of the surface oxide (cm^3 mol^{-1})
Z	Electrode impedance (Ω cm^2)
Z_{imag}	Imaginary part of the impedance (Ω cm^2)
Z_{real}	Real part of the impedance (Ω cm^2)
α	CPE power
ε	Dielectric constant of the film
ε_o	Dielectric constant of vacuum (8.85×10^{-14} F cm^{-1})
δ_{SC}	Space charge thickness (nm)
Δm	Mass-change sensitivity (ng Hz^{-1})

Ž. Petrović · M. Metikoš-Huković (✉) · R. Babić
Department of Electrochemistry,
Faculty of Chemical Engineering and Technology,
University of Zagreb,
PO Box 177, 10000 Zagreb, Croatia
e-mail: mmetik@fkit.hr

N. Lajçi
Faculty of Mines and Metallurgy, University of Prishtina,
MIP Trepca
40000, Mitrovica, Republic of Kosova

γ	Charge fraction
ω	Angular frequency (Hz)
ν	Scan rate (mV s^{-1})

Introduction

The properties of chromium passive films are of great technological importance because chromium is one of the major constituents in stainless steels [1], nickel-base alloys [2], and cobalt-base alloys [3, 4]. Because the corrosion resistance of these alloys is strongly dependent on the chromium content in the alloy substrate, a thorough understanding of the electrochemical behavior of passivity on chromium is of major interest. It is generally accepted that the passivation of chromium in H_2SO_4 is due to the formation of chromium (III) oxide-hydroxide [5–12], which occurs as a solid state process [13, 14]. However, no general agreement exists regarding the composition and electrochemical properties of passive films formed on Cr in acidic aqueous solutions. On the bases of ex situ spectroscopic studies, the passive film was identified as Cr_2O_3 [15] or CrOOH [5, 8]. Sunseri et al. [9], on the basis of in situ photocurrent technique, have reported that pure Cr_2O_3 cannot exist in the passive film on Cr at any pH value in aqueous solutions. They have suggested the formation of $Cr(OH)_3$ as a preliminary step, which transforms to less-hydrated Cr(III) oxide during the passive film growth; the formation of CrOOH has been suggested at higher anodic potentials and at low pH values. A bilayer structure of a passive film on Cr in H_2SO_4 was reported by several authors [11, 16, 17]. The XPS and STM studies on Cr in H_2SO_4 performed by Maurice et al. [11] have shown that $Cr(OH)_3$ forms first, and upon increasing potential and time of passivation an anhydrous Cr_2O_3 or less-hydrated CrOOH film forms underneath. Photoelectrochemical studies performed by Fujimoto et al. [16] and Tsuchiya et al. [17] on Cr and Fe-Cr alloy in H_2SO_4 have confirmed a bilayer structure of passive films on these substrates.

Because the semiconducting properties of passive films are linked to pitting nucleation, transpassive dissolution onset potential, and the corrosion potentials of metals, their deep understanding is important in determining the long-term corrosion properties of metals and alloys [18 and references therein]. However, the literature data show that the measured values of the electronic properties of the semiconductive nature of the passive films on chromium in H_2SO_4 obtained using photoelectrochemical and capacitance studies vary widely. The thermally grown passive films behave as a p-type semiconductor [19], while films formed in aqueous solutions can have either p- or n-type character. Several authors have reported that in the passive potential region the films on Cr behave as a p-type semiconductor due to chromium vacancies as the predominant point defects [9, 19–21], while at higher anodic potentials they show an n-type behavior related to the transpassive transformation [10, 20, 22]. On the basis of capacitance measurements, Tsuchiya et al. [17] have found that passive Cr in H_2SO_4 behaves as an n-type semiconductor in a wide potential region (0–600 mV vs. Ag/AgCl). They have attributed the n-type character to an outer hydroxide layer. More recent capacitance studies performed by Harrington and Devine [18] have shown that passive Cr in borate buffer behaves as an n-type semiconductor at 250 mV vs. standard hydrogen electrode (SHE). This behavior was attributed to the inner CrOOH barrier layer.

The aim of the present work was to investigate the passive film on Cr by using chronoamperometry, electrochemical impedance spectroscopy (EIS), Mott-Schottky, and electrochemical quartz crystal nanobalance (EQCN) methods. Investigations were performed in 0.5 M H_2SO_4.

Experimental

Solutions and electrodes

An aqueous solution of 0.5 mol dm^{-3} H_2SO_4; pH 0.4 (Fluka, p.a.) was prepared with distilled water. A mirror polished chromium-coated quartz crystal piezoresonator, (QC-10-CrB; A=0.196 cm^2), obtained from Elchema, was used as a working electrode and labeled as a Cr-QC electrode. It was degreased in absolute ethanol and deionized water before electrochemical measurements.

Electrochemical measurements

All experiments were carried out at room temperature in a standard three electrode cell. The counter electrode was a large area platinum electrode and the reference electrode, to which all potentials in the paper are referred, was an Ag|AgCl|3 M KCl (209 mV vs. SHE). For all experiments, the deoxygenation of the solution was ensured by the flow of N_2 (99.99%) 30 min prior to the experiment through the solution and above it during the measurements.

Cyclic voltammograms were recorded by sweeping the electrode potential from −0.7 V to anodic limit of 0.9 V and back with a sweep rate ν=50 mV s^{-1}. The potentiostatic current-time transients were recorded by applying a potential pulse from −0.2 V to various film formation potentials (E_f) ranging from 0.1 to 0.6 V, at which the electrode was polarized for 30 min. The samples passivated in this way were used in EIS measurements, which were performed with a voltage amplitude ±5 mV using a Solartron frequency response analyzer SI 1260 and Solartron

electrochemical interface 1287 controlled by a PC. The frequency range of the EIS data presented in the paper is between 10^5 Hz and 50 mHz. However, the preliminary measurements have shown that the log Z vs. log f dependence corresponding to the capacitive behavior of the electrode did not change until the low frequency limit of 5 mHz. The capacitance values of the Cr|solution interface, needed for a Mott-Schottky analysis, were determined from the imaginary part of impedance (Z_{imag}). It was recorded as a function of the potential at a frequency of 2 kHz. The potential was swept from E_f in the negative direction at a voltage sweep rate of 50 mV s^{-1}. Prior to each measurement the electrodes were stabilized for 2 h at the E_f.

The EQCN measurements were conducted using a system consisting of Elchema Potentiostat/Galvanostat, Model PS-205B and Electrochemical Quartz Crystal Nanobalance Elchema EQCN-700 with accompanied Faraday cage Elchema EQCN-702-2. A real-time Data Logger and Control system DAQ-716v with VOLTSCAN 5.0 acquisition and processing software were used for simultaneous recording of I–E and Δf–E, or Δm–E curves. The mass-change (Δm), sensitivity of 0.876 ng Hz^{-1}, was determined on the basis on the Sauerbrey's equation [23]. A polarization was started with a cathodic reduction at −0.5 V for 60 s and subsequently, the potential was set in the low passive region to −0.2 V, where the sample was kept for 15 min. Then, a potential pulse was applied to various film formation potentials, at which the EQCN measurements were performed during the 30-min time periods.

Results and discussion

Cyclic voltammetry

Figure 1 shows the cyclic voltammogram (CV) recorded on the Cr-QC electrode in 0.5 M H_2SO_4. The CV feature in Fig. 1 is in agreement with literature data [6, 10, 11, 24]. A sharp active–passive transition occurring at −0. 54 V can be observed only on the first CV. The chromium passivity attributes to the formation of protecting Cr(III) oxide, which is more or less hydrated. Because Cr(III) oxide is difficult to reduce electrochemically, the anodic current peak decreases during the repetitive cycling. A slight increase in the passive current with increasing anodic polarization can be observed. A current increase at higher anodic potentials (E>0.4 V) is due to the generation of chromium (VI) species in the passive film [6]. At a higher sweep rate and less anodic potential limits, as in the present study, accumulation of Cr(VI) species is very small and the cathodic current peak at around 0.7 V, corresponding to the reduction of Cr(VI) species, is slightly visible. The cathodic current increase at ca. −0.4 V is due to hydrogen adsorption and evolution.

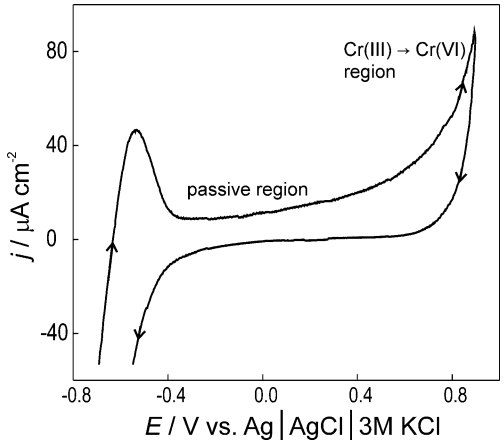

Fig. 1 The cyclic voltammogram of Cr recorded in 0.5 M H_2SO_4: ν= 50 mV s^{-1}

In situ gravimetry of anodic film formation on chromium

The parallel use of EQCN measurements with other techniques like voltammetry offers a very sensitive method for the in situ study the anodic film formation and growth on the metal surface [25–27]. In the present study, the mass change and the current change were recorded simultaneously during the surface film growth on the Cr-QC electrode under potentiostatic conditions. The mass increase registered during potentiostatic polarization is attributed to the formation of chromium oxide on the electrode surface. As an example, the insert in Fig. 2 presents the mass increase registered on the Cr-QC electrode at 0.2 V.

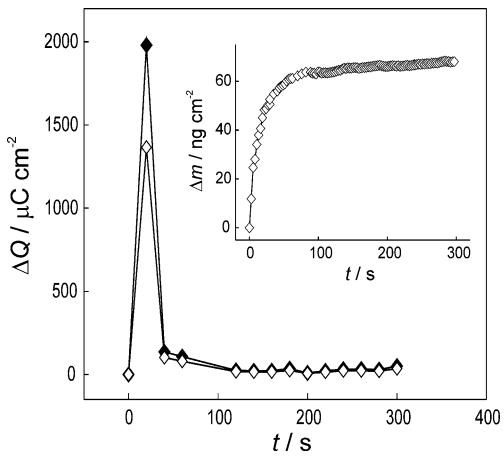

Fig. 2 The anodic charge (*black diamond*) and the charge consumed for the oxide film formation (*white diamond*) in denoted time intervals of potentiostatic polarization of Cr at 0.2 V in 0.5 M H_2SO_4. The *insert*: The mass response recorded during the simultaneous potentiostatic polarization

EQCN capability of simultaneous measuring of the changes in mass and current enables obtaining instantaneous mass/charge ratios ($F\mathrm{d}m/\mathrm{d}Q$ function) defined as [26, 27]:

$$F\frac{\mathrm{d}m}{\mathrm{d}Q}=\sum_{\mathrm{i}}\frac{M_{\mathrm{i}}}{n_{\mathrm{i}}}\gamma_{\mathrm{i}} \tag{1}$$

where M_{i} is the molar mass of a species i, which interchanges n_{i} electrons, γ_{i} is the charge ratio due to process i, and F is the Faraday constant. To analyse the $F\mathrm{d}m/\mathrm{d}Q$ function, the following processes are observed:

Cr dissolution:

$$\mathrm{Cr}\rightarrow \mathrm{Cr}^{3+}+3\mathrm{e}^{-},\quad F\mathrm{d}m/\mathrm{d}Q_{\mathrm{diss}}=-17.3\ \mathrm{g\ mol}^{-1} \tag{2}$$

and Cr passivation:

$$\mathrm{Cr}+2\mathrm{H_2O}\rightarrow \mathrm{CrOOH}+3\mathrm{H}^{+}+3\mathrm{e}^{-}\quad F\mathrm{d}m/\mathrm{d}Q_{\mathrm{pass}}=11\ \mathrm{g\ mol}^{-1} \tag{3}$$

with corresponding charge fractions γ_1 and γ_2 due to reactions (2) and (3), respectively. Thus, Eq. 1 can be rearranged:

$$F\frac{\mathrm{d}m}{\mathrm{d}Q}=-17.3\gamma_1+11\gamma_2 \tag{4}$$

$$\gamma_1+\gamma_2=1 \tag{5}$$

Using the experimentally determined values of $F\mathrm{d}m/\mathrm{d}Q$ ratio, which ranged from 2.20 to 4.20 g (mol e)$^{-1}$ over the time interval 0–30 min, the charge fractions γ_1 and γ_2 were calculated as a function of polarization time. The values of γ_2, equal to 0.73±0.03, indicate that the greater part of the total charge is used for the passive layer formation. The charge fraction γ_2 allows estimating the partial current densities corresponding to the film growth, i.e., the values of j_{CrOOH} ($j_{\mathrm{CrOOH}}=j\times\gamma_2$). These values can be used in determining the anodic charge Q_{CrOOH} corresponding to the oxide layer formation:

$$Q_{\mathrm{CrOOH}}(t)=\int_{t=0}^{t} j_{\mathrm{CrOOH}}\mathrm{d}t \tag{6}$$

The values of anodic charge (Q) and part of it consumed for the oxide formation (Q_{CrOOH}) in denoted time intervals of potentiostatic polarization are presented in Fig. 2.

The film thickness at any time t of the film growth can be calculated using the relation:

$$L_{\mathrm{ss}}=(Q_{\mathrm{CrOOH}}M_{\mathrm{CrOOH}})/(nF\rho_{\mathrm{CrOOH}}A) \tag{7}$$

where ρ is the density of CrOOH 4.01 g cm^{-3} [28]. At the time interval of 30 min, the charge consumed for oxide formation is equal to 3.08 mC cm^{-2} and the corresponding film thickness amounts to 2.2 nm.

The diffusivity of point defects within the growing anodic barrier film

A set of potentiostatic transients recorded in the potential range of anodic film formation and growth is presented in Fig. 3. An independency of the passive current density (j_{ss}) on the formation potential can be seen from the plot of ln j_{ss} vs. E_{f} presented in the inset of Fig. 3. According to the point defect model (PDM) [29–31], an independency of ln j_{ss} on E_{f} indicates that the barrier oxide layer on Cr behaves as an anion conductor due to a preponderance of anion vacancies over cation vacancies. According to the PDM, the flux of oxygen vacancies through the growing barrier films is essential to the film growth process [29–31]. Based on the Nernst-Planck transport equation, Sikora et al. [32] have demonstrated that the diffusivity of oxygen vacancies can be determined from the expression:

$$D_{\mathrm{O}}=-J_{\mathrm{O}}RT/2Fw_2H \tag{8}$$

where J_{O} is the steady state flux of oxygen vacancies, w_2 is the experimental parameter, H is the mean electric field strength (4.6×10^{6} V cm^{-1}), F is the Faraday constant (96,500 C mol^{-1}), while R and T have their usual meanings. The steady state flux of double-charged oxygen vacancies can be determined from the steady state passive current density; $J_{\mathrm{O}}=-j_{\mathrm{ss}}/2\mathrm{e}$, where e is the charge of an electron.

The steady state current density, $j_{\mathrm{ss}}=2.7\times10^{-7}$ A cm^{-2}, determined from potentiostatic transients, gave the value of J_{O} equal to 8.5×10^{11} s^{-1} cm^{-2}. Because the value of w_2 is of the same order of magnitude as N_{D} [32, 33], the value

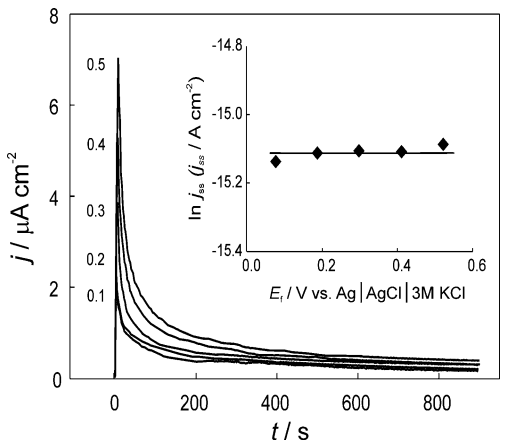

Fig. 3 The potentiostatic transients of Cr recorded in 0.5 M H_2SO_4. The *insert*: The dependence of the steady-state passive current density on the film formation potential

of N_D determined from Mott-Schottky analysis (1.8×10^{20} cm^{-3}) was used in a rough estimation of D_O. The substitution of the above values into Eq. 8 gave the value for D_O equal to 1.3×10^{-17} cm^2 s^{-1}. This value agrees well with D_O calculated from initial periods of potentiostatic transients (Fig. 3) on the basis of the Cottrell equation. The value of the same order was reported by Vazquez et al. [33] for anodic WO_3 films in 0.1 M $HClO_4$. The values of D_O calculated using the low-field limit are approximately two orders of magnitude higher than those calculated using the high-field limit approximation [33, 34].

Impedance measurements on passivated chromium electrode

Impedance spectra were recorded on passive chromium in 0.5 M H_2SO_4 at film formation potentials ranging from 0.2 to 0.6 V. The spectra are presented in Fig. 4 as Bode plots. It is evident that the passive Cr electrode shows almost ideal capacitive behavior inside a broad frequency region in which the slope of the log $|Z|$ against log f straight lines is close to −1 and the phase angle approaches −90°. Preliminary measurements have shown that the region where the current and potential are in phase, i.e., the low frequency dc limit was not reached at the low frequency limit of 5 mHz, at which the impedance magnitude value was about 10^6 Ω cm^2. All these facts indicate that the passive chromium electrode behaves as a blocking electrode, which can be represented with an equivalent circuit (EEC) of a capacitance in series with an ohmic resistance. The justification for the application of a blocking circuit in representing the EIS data for passive Cr was tested on the basis of the dependence of imaginary part of the complex capacitance (C_{imag}) on frequency [35].

Figure 5 shows the $-C_{imag}$ vs. f dependence in a logarithmic scale, which is typical for a blocking electrode. However, it is well known that the impedance results for a solid electrode|electrolyte interface often reveal a frequency dispersion that cannot be described by simple electrical elements [36]. The frequency dispersion, generally attributed to the "capacitance dispersion", can be eliminated for the passive films by replacing the capacitor in the electrical equivalent circuit with the constant phase element (CPE). The impedance of the CPE has the form:

$$Z(\mathrm{CPE}) = [Q(j\omega)^{\alpha}]^{-1} \tag{9}$$

where Q is the constant, ω is the angular frequency, and α is the CPE power. Therefore, the impedance of the blocking electrodes represented by a CPE in series with an electrolyte resistance is given by [37]:

$$Z(f) = R_{el} + 1/(j2\pi f)^{\alpha}Q \tag{10}$$

where R_{el} is the electrolyte resistance, and parameters α and Q are associated with a CPE.

The spectra were analyzed using the software for complex-linear least squares [38]. The values of α and Q are presented in Table 1. The error in calculation of particular components less than 5% justifies the presentation of passive Cr as a blocking electrode.

The numerical values of interfacial capacitance C of passive chromium electrode at various E_f was calculated using the Brug's expression [39]:

$$C = \left(QR_{el}^{1-\alpha}\right)^{1/\alpha} \tag{11}$$

where R_{el} is the electrolyte resistance ($R_{el} = 13.27\pm 0.06$ Ω cm^2). The values obtained show that the capacitance of passive Cr is almost constant inside the potential

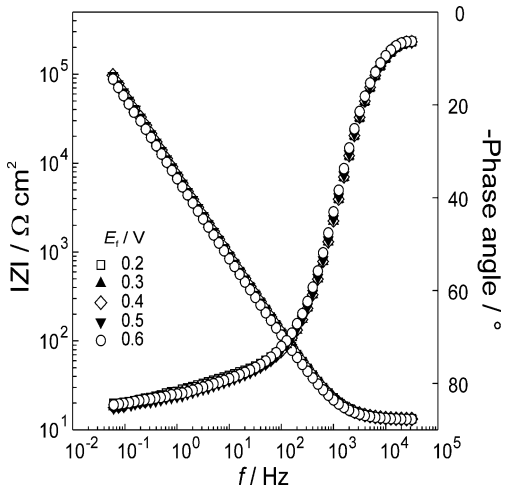

Fig. 4 The *Bode plot* representation of the impedance spectra of Cr passivated at denoted potentials in 0.5 M H_2SO_4

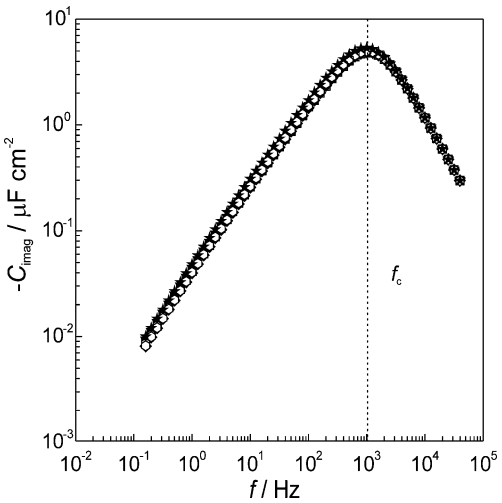

Fig. 5 The imaginary part of the complex capacitance on a logarithmic plot as a function of frequency for passive Cr in the potential region from 0.2 to 0.6 V

Table 1 The impedance parameters obtained for passive Cr in 0.5 M H_2SO_4. The electrode capacitance was calculated according to the Brug's equation

E_f/V	α	$Q\times10^6/\Omega^{-1}$ cm^{-2}s$^{\alpha}$	C/μF cm^{-2}
0.2	0.889	27.9	10.4
0.3	0.890	26.6	10.2
0.4	0.893	25.9	9.96
0.5	0.895	26.1	10.0
0.6	0.891	28.7	11.2
0.7	0.875	37.7	12.9

region up to 0.5 V and increases at higher E_f values, at which the Cr(III) to Cr(VI) oxidation takes place.

The semiconducting properties of the passive film on chromium

The most common in situ method for probing the semiconducting properties of passive films is Mott-Schottky analysis of the electrode capacitance vs. potential dependence [40, 41]. To obtain the electrode capacitance, the Z_{imag} of the passivated Cr electrode at a particular anodic potential was measured by sweeping the potential to the cathodic direction at a constant frequency (2 kHz). From the measured values of Z_{imag} and the previously determined CPE exponent α (Table 1) it was possible to calculate the CPE parameter Q, and then the electrode capacitance by using the Brug's equation (Eq. 11). Assuming that the capacitance of the Helmholtz layer can be neglected, the capacitance determined is equal to the 'space charge' capacitance. According to the Mott-Schottky theory [41], the space charge capacitance of an n-type semiconductor is given by:

$$\frac{1}{C_{SC}{}^2} = \frac{2}{\varepsilon\varepsilon_0 e N_D}\left(E - E_{fb} - \frac{kT}{e}\right) \tag{12}$$

where N_D is the donor concentration in the passive film, E is the applied potential, E_{fb} is the flat-band potential, e is the electron charge (1.602×10^{-19} C), and k is the Boltzman constant (1.38×10^{-23} J K^{-1}). For n-type semiconductors, the C^{-2} versus E dependence should be linear with a positive slope that is inversely proportional to the donor concentration.

The C^{-2} vs. E profiles, recorded for films formed on chromium in 0.5 M H_2SO_4 at specified formation potentials, are presented in Fig. 6. The linear C^{-2} vs. E dependence with a positive slope, observed over a potential region of about 500 mV, is characteristic of n-type semiconductors. The donor concentration, calculated using Eq. 12, is equal to 1.8×10^{20} cm^{-3}, indicating that the oxide layer behaves like the heavily doped semiconductors.

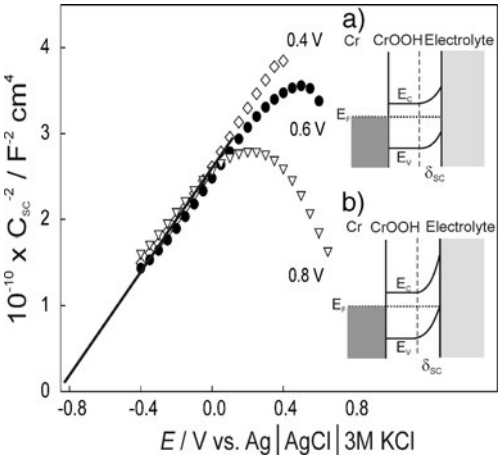

Fig. 6 The Mott-Schottky plot of Cr passivated at denoted potentials in 0.5 M H_2SO_4. The *insert*: The schematic presentation of the electronic energy-band model for passive Cr in 0.5 M H_2SO_4

However, it has been shown by de Gryse et al. [42] that the slope of the Mott-Schottky plot is retained in heavily doped semiconductors and can still be used to derive reliable values of N_D in contrary to the determination of the flat-band potential values. The values of N_D obtained in the present work agree well with that reported for Cr in borate buffer, pH=8.4 [18]. For passive Cr in 0.1 M H_2SO_4 Tsuchiya et al. [17] reported the value of N_D of the order of magnitude of 10^{21} cm^{-3}.

The space charge thickness (δ_{SC}) has been calculated using the relationship [43]:

$$\delta_{SC} = \left(2\varepsilon\varepsilon_0(E - E_{fb})/eN_D\right)^{0.5} \tag{13}$$

With the E_{fb} values equal to −0.83 V vs. Ag/AgCl, the values of δ_{SC} corresponding to passive films inside the potential region 0.40–0.80 V are equal to 4.1 nm.

Although the flat-band potential values cannot be accurately determined from the Mott-Schottky plot for heavily doped semiconductors, Fig. 6 shows that its value is cathodic with respect to potentials of the passive region. By applying an anodic polarization to the passive electrode, the Fermi level of the metal lowers inducing an electron band banding upwards in the film, while the Helmholtz layer potential difference remains constant. This mode of potential distribution is maintained as long as the Fermi level remains within the forbidden band of the film as shown by a schematic presentation given in the insert (a) in Fig. 6. At very high anodic potentials ($E\geq0.60$ V), the upper valence band edge reaches the Fermi level (the insert (b) in Fig. 6), and the hole charge carriers accumulate in the outermost surface layer of the passive film. As a consequence, the electrode capacitance increases and, for example, at 0.8 V it equals to 30 μF cm^{-2}. The increase in anodic potential accompanied with increasing Helmholtz layer potential difference accelerates the rate of dissolution

of passive Cr, which proceeds with an increase in the oxidation state of Cr. This mode of oxidative dissolution is a hole (h)—accepting reaction:

$$2CrOOH + 6h + 3H_2O \rightarrow Cr_2O_7^{2-} + 8H^+ \quad (14)$$

Conclusion

A description of the steady-state oxide film, formed on Cr under potentiostatic conditions in 0.5 M H_2SO_4, as a thin barrier layer with a small intrinsic conductivity and as the depletion layer close to the film|electrolyte interface was consistent with experimental results of EIS. The frequency dispersion of the passivated Cr electrode was addressed by replacing the interfacial capacitance with a CPE in the EEC of the investigated system. The effective capacitance C of a CPE measured by EIS and Mott-Schottky analysis was determined according to the Orazem's and Brug's expressions.

The Nernst-Planck transport equation for low-field limit approximation and Mott-Schottky analysis were used to identify the stoichiometric defects, the majority charge carriers in the passive film on Cr as well as its electronic structure. The anion diffusion coefficient was extracted from the relationship between the donor density and the film formation potential assuming that the depletion region in the film close to the film|electrolyte interface dominates semiconductor properties. According to the Mott-Schottky analysis, the passive film on Cr in acid solution behaves as an n-type semiconductor. The anion vacancies formed during oxide film growth act as electron donors.

Acknowledgement The financial support of the Ministry of Science, Education and Sports of the Republic of Croatia under the 125-0982904-2923 grant is gratefully acknowledged.

References

1. Babić R, Metikoš-Huković M (1993) J Electroanal Chem 358:143–160
2. Metikoš-Huković M, Omanović S, Babić R, Milošev I (1994) Ber Bunsenges Phys Chem 98:1243–1249
3. Metikoš-Huković M, Babić R (2009) Corros Sci 51:70–75
4. Metikoš-Huković M, Pilić Z, Babić R, Omanović D (2006) Acta Biomater 2:693–700
5. Asami K, Hashimoto K, Shimodaira S (1978) Corros Sci 18:151–160
6. Moffat TP, Latanision RM (1992) J Electrochem Soc 139:1869–1879
7. Moffat TP, Yang H, Fan FRF, Bard AJ (1992) J Electrochem Soc 139:3158–3167
8. Sugimoto K, Matsuda S (1980) Mat Sci Eng 42:181–189
9. Sunseri C, Piazza S, DiQuatro F (1990) J Electrochem Soc 137:2411–2417
10. Bojinov M, Fabricius G, Laitinen T, Saario T, Sundholm G (1998) Electrochim Acta 44:247–261
11. Maurice V, Yang WP, Marcus P (1994) J Electrochem Soc 141:3016–3027
12. Kim H, Hara N, Sugimoto K (1999) J Electrochem Soc 146:3679–3685
13. Haupt S, Strehblow H-H (1987) J Electroanal Chem 228:365–392
14. Dobbelaar JAL, De Wit JHW (1990) J Electrochem Soc 137:2038–2046
15. Seo M, Saito R, Saito N (1980) J Electrochem Soc 127:1909–1912
16. Fujimoto S, Chihara O, Shibata T (1998) Mat Sci Forum 289–292:989–996
17. Tsuchiya H, Fujimoto S, Chihara O, Shibata T (2002) Electrochim Acta 47:4357–4366
18. Harrington SP, Devine TM (2009) J Electrochem Soc 156:C154–C159
19. Metikoš-Huković M, Ceraj-Cerić M (1987) J Electrochem Soc 134:2193–2197
20. Kim J, Cho E, Kwon H (2001) Electrochim Acta 47:415–421
21. Kong D-S, Chen S-H, Wang C, Yang W (2003) Corros Sci 45:747–758
22. Searson PC, Latanision RM (1990) Electrochim Acta 35:445–450
23. Sauerbrey G (1959) Z Phys 155:206–222
24. Gerretsen JH, De Wit JHW (1990) Corros Sci 30:1075–1084
25. Olsson COA, Hamm D, Landolt D (2000) J Electrochem Soc 147:2563–2571
26. Gregori J, Garcia-Jareno JJ, Vincente F (2006) Electrochem Commun 8:683–687
27. Gregori J, Garcia-Jareno JJ, Gimenez-Romero D, Vincente F (2006) Electrochim Acta 52:658–664
28. Weast RC (1962) Handbook of chemistry and physics. The Chemical Rubber Co., Cleveland
29. Macdonald DD, Urquidi-Macdonald M (1990) J Electrochem Soc 137:2395–2399
30. Macdonald DD (1992) J Electrochem Soc 139:3434–3449
31. Liu J, Macdonald DD (2001) J Electrochem Soc 148:B425–B430
32. Sikora E, Sikora J, Macdonald DD (1996) Electrochim Acta 41:783–789
33. Vasquez G, Gonzales I (2007) Electrochim Acta 52:6771–6777
34. Bojinov M, Fabricius G, Laitinen T, Makela K, Saario T, Sundholm G (2001) Electrochim Acta 46:1339–1358
35. Orazem ME, Tribollet B (2008) Electrochemical impedance spectroscopy. John Wiley & Sons. Inc., New Jersey
36. Jorcin J-B, Orazem ME, Pebere N, Tribollet B (2006) Electrochim Acta 51:1473–1479
37. Orazem ME, Pebere N, Tribollet B (2006) J Electrochem Soc 153: B129–B136
38. Boukamp BA (1986) Solid State Ionics 18–19:136–140
39. Brug GJ, van der Eeden ALG, Sluyters-Rehbach M, Sluyters JH (1984) J Electroanal Chem 176:275–295
40. Sikora E, Macdonald DD (1997) Solid State Ionics 94:141–150
41. Morrison SR (1980) Electrochemistry at semiconductor and oxidized metal electrodes. Plenum Press, New York
42. De Gryse N, Gomes P, Cardon F, Vennik J (1975) J Electrochem Soc 122:711–712
43. Metikoš-Huković M, Omanović S, Jukić A (1999) Electrochim Acta 45:977–986